

Article

Unveiling the Exceptional Performance of ZnO/Zn₂TiO₄ Nanocomposites

Husnain Ahmad Abbasi¹, Maha M. Al Moneef^{2,*} , Jahanzeb Khan³ , Muhammad Hafeez^{1,*}, Muhammad Usman Hameed⁴, Muhammad Abdullah Khan⁵ , Shabnam Shahida⁴, Habib Ahmad Abbasi⁶ and Sook-Keng Chang⁷ 

- ¹ Department of Chemistry, University of Azad Jammu and Kashmir, Azad Kashmir, Muzaffarabad 13100, Pakistan
- ² Department of Physics, College of Science, Princess Nourah Bint Abdulrahman University, Riyadh 11671, Saudi Arabia
- ³ Department of Chemistry, Mirpur University of Science and Technology (MUST), Azad Kashmir, Mirpur 10250, Pakistan
- ⁴ Department of Chemistry, University of Poonch Rawalakot, Rawalakot 12350, Pakistan
- ⁵ Department of Environmental Sciences, Quid-i-Azam University, Islamabad 45320, Pakistan
- ⁶ Department of Physics, University of Azad Jammu and Kashmir, Azad Kashmir, Muzaffarabad 13100, Pakistan
- ⁷ Faculty of Health and Life Sciences, INTI International University, Persiaran Perdana BBN, Putra Nilai, Nilai 71800, Negeri Sembilan, Malaysia
- * Correspondence: mmalmoneef@pnu.edu.sa (M.M.A.M.); muhammadhafeezchemist@gmail.com (M.H.)

Abstract: In this study, we engineered a sub-70 nm nanocomposite of ZnO/Zn₂TiO₄ using a low-temperature solution-phase method with titanium isopropoxide and zinc acetate as precursors, and isopropyl alcohol and water as solvents. The investigation focused on nanocomposite growth by varying precursor and surfactant concentrations and their efficiency within different pH ranges. All three ZnO/Zn₂TiO₄ nanocomposites exhibited hexagonal wurtzite ZnO and Zn₂TiO₄ structures. The crystallite size in these nanocomposites ranged from 39.50 nm to 62.67 nm for ZnO and 21.24 nm to 26.15 nm for Zn₂TiO₄. Morphological observations using FESEM revealed the formation of dispersed cotton packet-like nanocomposites with sizes ranging from 18 to 350 nm. FTIR analysis showed peaks indicative of Ti–O and Zn–O bond formation, and EDX spectrum confirmed the presence of Ti, O, and Zn. UV spectra and photocatalytic investigations confirmed the successful formation of ZnO/Zn₂TiO₄ nanocomposites with notable photocatalytic degradation efficiency for methylene blue dye under various conditions. These findings suggest the potential applicability of the synthesized nanocomposites for environmental pollutant degradation.

Keywords: ZnO/Zn₂TiO₄ nanocomposites; spectrum; methylene blue; dye



Citation: Abbasi, H.A.; Al Moneef, M.M.; Khan, J.; Hafeez, M.; Hameed, M.U.; Khan, M.A.; Shahida, S.; Abbasi, H.A.; Chang, S.-K. Unveiling the Exceptional Performance of ZnO/Zn₂TiO₄ Nanocomposites. *Catalysts* **2024**, *14*, 156. <https://doi.org/10.3390/catal14020156>

Academic Editors: Andrei V. Shevelkov and Maxim N. Sokolov

Received: 10 December 2023

Revised: 29 January 2024

Accepted: 31 January 2024

Published: 19 February 2024



Copyright: © 2024 by the authors. Licensee MDPI, Basel, Switzerland. This article is an open access article distributed under the terms and conditions of the Creative Commons Attribution (CC BY) license (<https://creativecommons.org/licenses/by/4.0/>).

1. Introduction

Photocatalysis technology, conceived in the late 1960s as a solution for water and wastewater treatment, addresses the critical issue of water pollution primarily caused by organic pollutants, constituting over 50% of water contaminants [1]. The pervasive presence of toxic contaminants in water and wastewater poses serious threats to both human beings and aquatic life [1]. In this context, nanotechnology, involving the creation of nanostructures with dimensions between atoms and bulk atom materials, presents a transformative approach [2]. Photocatalysis, a technique utilizing photocatalysts and light irradiation for pollutant degradation, has become a cornerstone in energy generation and environmental restoration efforts [3,4]. The global expansion of the population has heightened the demand for clean water, with billions of people experiencing freshwater scarcity [5,6]. In recent years, mixed metal oxide additives have gained attention for their unique properties and diverse applications in various fields [1]. Comprising different metal

oxides, these additives enhance material performance, improving mechanical, electrical, and catalytic properties. Their tunable properties, achieved by varying composition and ratio, offer versatility for applications in industries such as energy storage, electronics, and environmental remediation. Notably, mixed metal oxide additives exhibit excellent stability and durability, making them suitable for long-term use in demanding conditions, with resistance to corrosion and high temperatures [1].

Synthesizing ZnO: Zn₂TiO₄ nanocomposite powder has been explored through various methods, including the co-precipitation method, sol-gel precipitating method, solid-state reaction, and solution combustion. Among these, the sol-gel precipitating method stands out for its prominence in synthesizing nanocrystalline materials, facilitating the formation of distinctive metastable structures at low reaction temperatures, ensuring excellent chemical consistency and the preparation of a high-purity, well-crystallized powder of nanocomposites [1]. Nanostructured Zn₂TiO₄ and zinc oxide (ZnO) are recognized n-type semiconductor materials with wide band gaps of approximately 3.22 eV and 3.37 eV, respectively. These materials play crucial roles in absorbing electromagnetic energy and degrading organic pollutants through photodegradation [1].

Despite their similar band gap energy values, Zn₂TiO₄ and ZnO exhibit distinct redox energy levels, making them suitable for the preparation of core-shell heterojunction nanostructures. Various synthesis methods, such as physical vapor deposition, microwave-assisted hydrothermal techniques, and radiofrequency sputtering, have been explored for ZnO/Zn₂TiO₄ heterostructures. However, achieving tunable structures through low-cost fabrication procedures remains a significant challenge, with co-precipitation standing out as a simple and cost-effective method widely used in industrial production [2].

ZnO/Zn₂TiO₄ boasts appealing properties, including excellent transparency in the visible spectrum, a high piezoelectric constant, a significant electro-optic coefficient, and a substantial excitation binding energy of approximately 60 meV at room temperature [7]. Significant efforts have been directed towards improving the photocatalytic performance of ZnO/Zn₂TiO₄ through various approaches, including doping with other ions, surface coupling with other semiconductors to form a heterojunction, photosensitization, and nanostructure design [8]. The unique combination of oxygen and metal in ZnO/Zn₂TiO₄ creates distinct characteristics, contributing to reactive electrical transitions and broad bandgaps [9,10]. Studies have explored the beneficial characteristics of ZnO nanostructures, dependent on the concentration of Zn₂TiO₄, showcasing their importance for semiconductors [11]. Several approaches, such as Zn function doping and light stimulation, have been investigated to enhance the performance of ZnO/Zn₂TiO₄ nanostructures. By employing methods that decrease bulk materials, including etching, breaking, or cutting, nanostructures with diverse morphologies have been successfully created, providing a “top-down” approach [12,13]. The nanocomposite demonstrates adaptability for photonic usage in the UV spectral region at room temperature due to its broad super lattice and high ionization potential energy of 60 meV [14].

ZnO, an affordable and harmless semiconductor material, maintains a higher level of chemical stability. Various nanostructures, including nanorods, nanobelts, nanorings, nanowires, and nanoflowers, have been synthesized to leverage its versatile properties [15–18]. The hydrothermal process has proven to be a useful strategy for producing ZnO nanostructures and other luminescent materials [19]. Exhibiting ionicity between ionic and covalent materials, ZnO has distinct crystal formations such as wurtzite, zinc blende, and rock salt. ZnO wurtzite structure, frequently thermodynamically stable in natural settings, exhibits unique arrangements of Zn and O ions in tetrahedrons, resulting in an asymmetric structure with surfaces carrying positive or negative charges [20,21]. ZnO finds various technical uses, including in heterogeneous catalysis and optoelectronics, emphasizing the critical importance of understanding its band structure for potential effects in devices and improving their functionality [14]. Research groups have explored dual core-shell nanostructures to enhance the photocatalytic performance of metal oxide semiconductor nanomaterials. For instance, Kwiatkowski et al. prepared ZnO/Zn₂TiO₄ core/shell composites through

sol–gel deposition, demonstrating their efficacy in the photodecomposition of methylene blue [3]. Experimental techniques, such as X-ray-induced photoabsorption and photoemission spectroscopy, are commonly employed to recognize the band structure of ZnO, providing insights into its optoelectronic characteristics [22].

Understanding the ZnO band structure is crucial, considering its equal valence band and conduction band zones at $k = 0$, indicative of a straight band gap material with a wurtzite structure [23]. ZnO nanostructures exhibit photocatalytic properties that protect against bacteria, fungi, and viruses, making them valuable for degrading environmental pollutants. The generation of reactive oxygen species, catalytic activity using photosurfactants, and UV radiation-induced cancer damage all depend on ZnO nanostructures, a common excitation gap semiconductor [24]. The processing of higher exciton binding energies by ZnO/Zn₂TiO₄ results in efficient exciton emission at ambient temperature and visible spectrum, in addition to the ultraviolet spectrum [25]. ZnO photoluminescence spectra typically show a UV band corresponding to (NBE) at room temperature and one or two visible bands consisting of defects, such as interstitial vacancies, extra atoms occupying lattice interstices, and complicated defects [26]. The use of large ZnO nanoparticles presents aesthetic challenges, and researchers have investigated the effects of cross-linking activity mechanisms on the size, surface, and morphology of ZnO [27,28]. Noteworthy applications of ZnO include its use as a relief agent for infant diaper rash and its inclusion in creams for cancer treatment to kill tumor cells while causing minimal harm to healthy cells [29]. Among various photocatalysts, Zn₂TiO₄ stands out as a widely employed “golden” photocatalyst, extensively used in heterogeneous photocatalysis due to its chemical stability, nontoxicity, and low cost [30,31]. The rapid growth of Zn₂TiO₄ heterogeneous photocatalysis in the past two decades has been driven by diverse energy and environmental challenges, including direct solar water splitting into H₂ and the decomposition of air pollutants and water at low concentrations [32]. The literature on heterogeneous photocatalysis has been extensively reviewed, addressing the development of photocatalysts, characterization of photocatalytic processes, and the challenges and opportunities confronting this field [33]. To the best of our knowledge, this work reports the first instance of enhanced photoreactivity in the ZnO/Zn₂TiO₄ nanocomposite.

2. Results and Discussion

2.1. Scanning Electron Microscopy (SEM) and Energy Dispersive X-ray Spectroscopy

Figure 1a–c show the microstructures of three ZnO/Zn₂TiO₄ nanocomposites. The ZnO/Zn₂TiO₄ nanocomposite structures were explained to have a magnitude of 200 nm which is displayed. The particle thickness in the three ZnO/Zn₂TiO₄ nanocomposites ranged in diameter from 18 to 350 nm. The size of the spherical nanocomposite in this study indicates the structure of the ZnO/Zn₂TiO₄ nanocomposites [34,35].

Using the EDX method, the elemental composition of sample materials was identified. Figure 1 shows the EDX spectrum for the three synthesized ZnO/Zn₂TiO₄ nanocomposites. The EDX spectrum shows peaks for different contents in the synthesized sample. The ZnO/Zn₂TiO₄ nanocomposite synthesis was confirmed by the presence of peaks for Zn, O, and Ti. Zn, O, and Ti make up a significant amount of the final products' weight, as seen by the spectra. In the three ZnO/Zn₂TiO₄ nanocomposites, element Zn has the weight percentage 49.44%, 48.03%, and 42.28%, while element Ti has the weight percentage 22.22%, 20.29%, and 23.26%. Also, element O has the weight percentage 25.8%, 31.69%, and 34.46%. An EDX examination shows the presence of the anticipated ZnO/Zn₂TiO₄ nanocomposite components with no additional impurities or elements discovered, demonstrating that the nanocomposites were properly manufactured. Zn, Ti, and O all are included, and their weight percentages almost exactly match the composition [36].

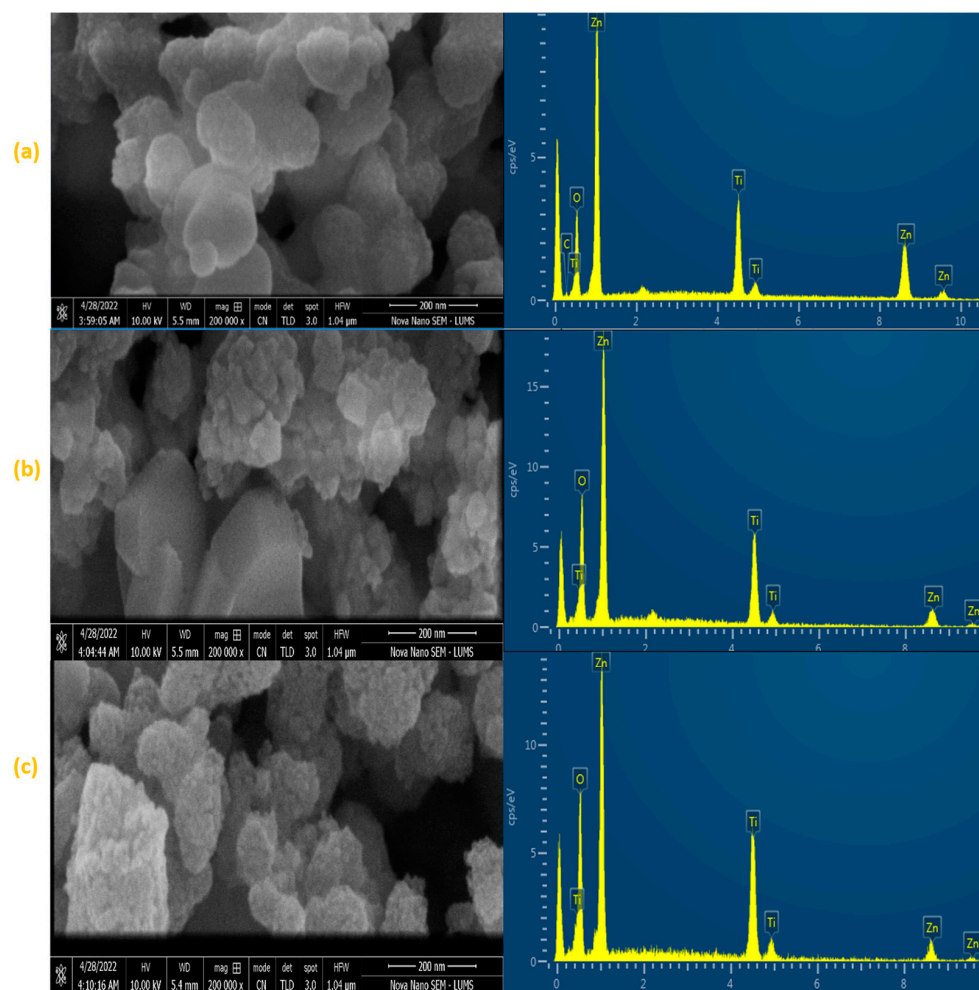


Figure 1. FESEM magnification micrograph and EDX analysis of synthesized ZnO–Zn₂TiO₄ nanocomposites: (a) 85% ZnO–15% Zn₂TiO₄ nanocomposite, (b) 75% ZnO–25% Zn₂TiO₄ nanocomposite, and (c) 65% ZnO–35% Zn₂TiO₄ nanocomposite.

2.2. X-ray Diffraction Analysis (XRD)

XRD confirms the hexagonal wurtzite ZnO and Zn₂TiO₄ of the three synthesized ZnO/Zn₂TiO₄ nanocomposites (Figure 2). Other reflections in the XRD pattern of the three synthesized ZnO/Zn₂TiO₄ nanocomposites have been observed at $2\theta = 31.98^\circ$, 34.56° , 36.45° , 42.75° , and 63.05° which are consistent with the Miller indices of (100), (002), (101), (102), and (110) representing ZnO (JCPDS (Joint Committee on Powder Diffraction Standards) card no: 36–1451) which nicely matched the observed peaks and showed that they are highly crystalline.

Also, there are peaks at 53.8° , 56.75° , and 69.90° which is consistent with the Miller indices of (020), (110), and (220) that correspond to the Zn₂TiO₄ phase (JCPDS card 25–1164). Furthermore, the grain sizes of the ZnO/Zn₂TiO₄ nanocomposites are determined using the Scherer formula.

$$D = \frac{0.9\lambda}{\beta \cos\theta} \quad (1)$$

where D is the average grain-size, which might be smaller or larger than grain size, β indicates full width at half maximum of the peak in radian, and ‘ θ ’ shows Bragg’s angle. In the ZnO/Zn₂TiO₄ nanocomposites, ZnO crystallite size values were 62.67, 40.34, and 39.50 nm. While the anatase phase size values were 26.15, 25.36, and 21.24 nm, respectively [35].

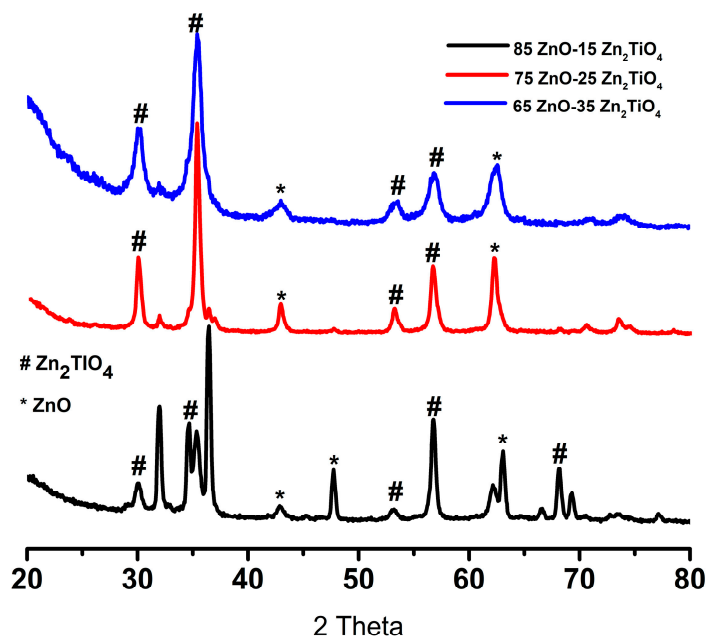


Figure 2. XRD pattern of synthesized ZnO/Zn₂TiO₄ nanocomposites: 85% ZnO–15% Zn₂TiO₄ nanocomposite, 75% ZnO–25% Zn₂TiO₄ nanocomposite, and 65% ZnO–35% Zn₂TiO₄ nanocomposite.

2.3. Fourier Transform Infrared Spectroscopy (FTIR)

A double beam spectrophotometer was used to analyze the chemically synthesized sample. Figure 3a shows the FTIR spectra of the ZnO/Zn₂TiO₄ nanocomposites, with peaks observed at 3413 cm⁻¹, 2070 cm⁻¹, 1639 cm⁻¹, 1381 cm⁻¹, and 1117 cm⁻¹. In Figure 3b, on the left, the FTIR spectra of the ZnO/Zn₂TiO₄ nanocomposites reveal peaks at 3442 cm⁻¹, 1629 cm⁻¹, 1404 cm⁻¹, 1116 cm⁻¹, and 611 cm⁻¹.

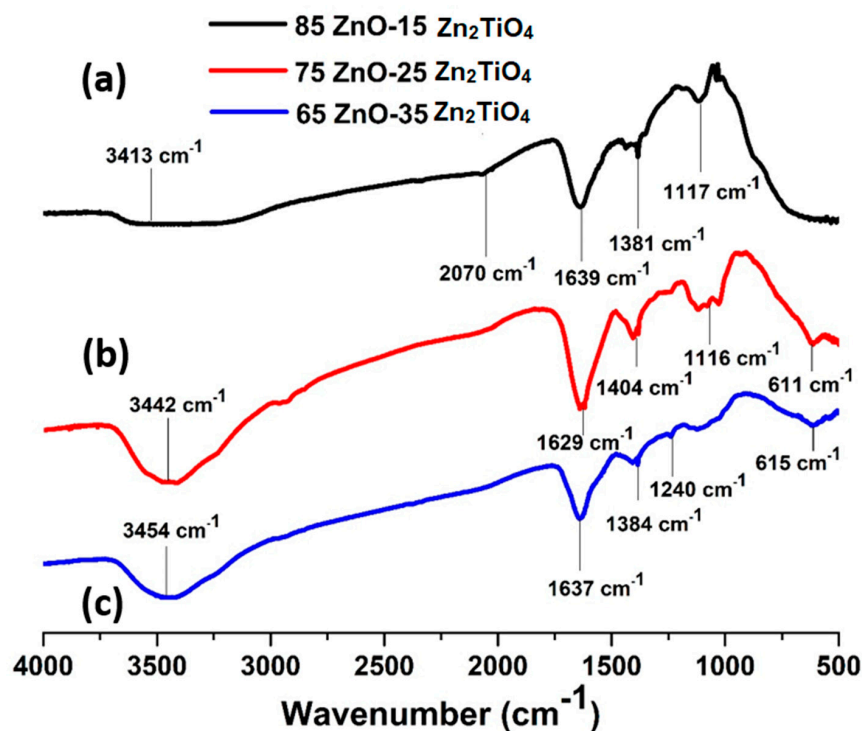


Figure 3. FTIR spectrum of ZnO–Zn₂TiO₄ nanocomposites: (a) 85% ZnO–15% Zn₂TiO₄ nanocomposite, (b) 75% ZnO–25% Zn₂TiO₄ nanocomposite, and (c) 65% ZnO–35% Zn₂TiO₄ nanocomposite.

Figure 3c at left displays the FTIR spectra of the ZnO/Zn₂TiO₄ nanocomposite in which the peaks at 3454 cm⁻¹, 1637 cm⁻¹, 1384 cm⁻¹, 1240 cm⁻¹, and 615 cm⁻¹ were obtained. Peaks in the range of 610–1250 cm⁻¹ are attributed to Ti–O bond formation. The peak at 3652–3170 cm⁻¹ represents the O–H bond. The peak at 1610–2335 cm⁻¹ is attributed to bending vibrations of the C=O molecule. The peaks located at 1350–1450 cm⁻¹ are attributed to Zn–O bond formation [37,38].

2.4. Ultra Violet–Visible Spectroscopy

Intense peaks are seen in the UV spectrum of the three ZnO/Zn₂TiO₄ nanocomposites. In Figure 4a, the synthesized ZnO/Zn₂TiO₄ nanocomposite showed absorbance at 345 nm and 251 nm. In Figure 4b, the synthesized ZnO/Zn₂TiO₄ nanocomposite showed absorbance at 341 nm and 285 nm, respectively. In Figure 4c, the synthesized ZnO/Zn₂TiO₄ nanocomposite showed absorbance at 354 nm and 288 nm. This is an indication of the fact that the synthesized ZnO/Zn₂TiO₄ nanocomposites are photosensitive in the UV region [39,40].

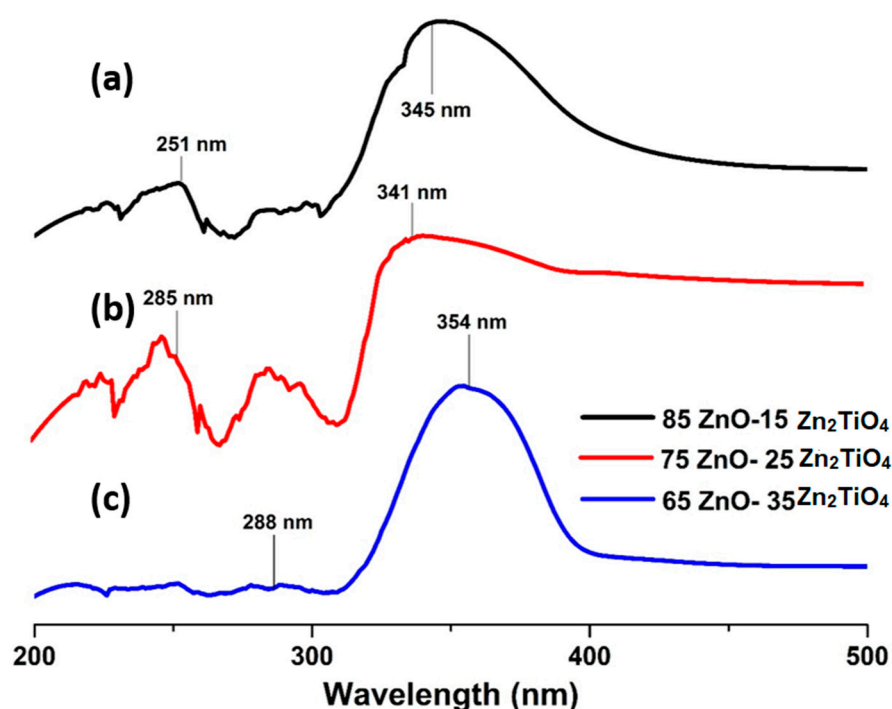


Figure 4. Ultraviolet–visible spectrum of ZnO–Zn₂TiO₄ nanocomposites: (a) 85% ZnO–15% Zn₂TiO₄ nanocomposite, (b) 75% ZnO–25% Zn₂TiO₄ nanocomposite, and (c) 65% ZnO–35% Zn₂TiO₄ nanocomposite.

2.5. Photocatalytic Activity

The photocatalytic activity of three ZnO/Zn₂TiO₄ nanocomposites was compared by using methylene blue dye as the model pollutant. Experiments used 20 mL of methylene blue solution with 2 mg of the catalyst suspended in it while being exposed to UV light. By stirring the reaction mixture for 30 min in the dark prior to irradiation, the adsorption–desorption equilibrium was achieved. Stirring the reaction mixture in the dark, there was no decrease in methylene blue concentration due to no absorption of the dye (MB) solution, but under light, passing time with repeated intervals of 20 min, absorbance was shown by the MB solution (as depicted in Figure 5).

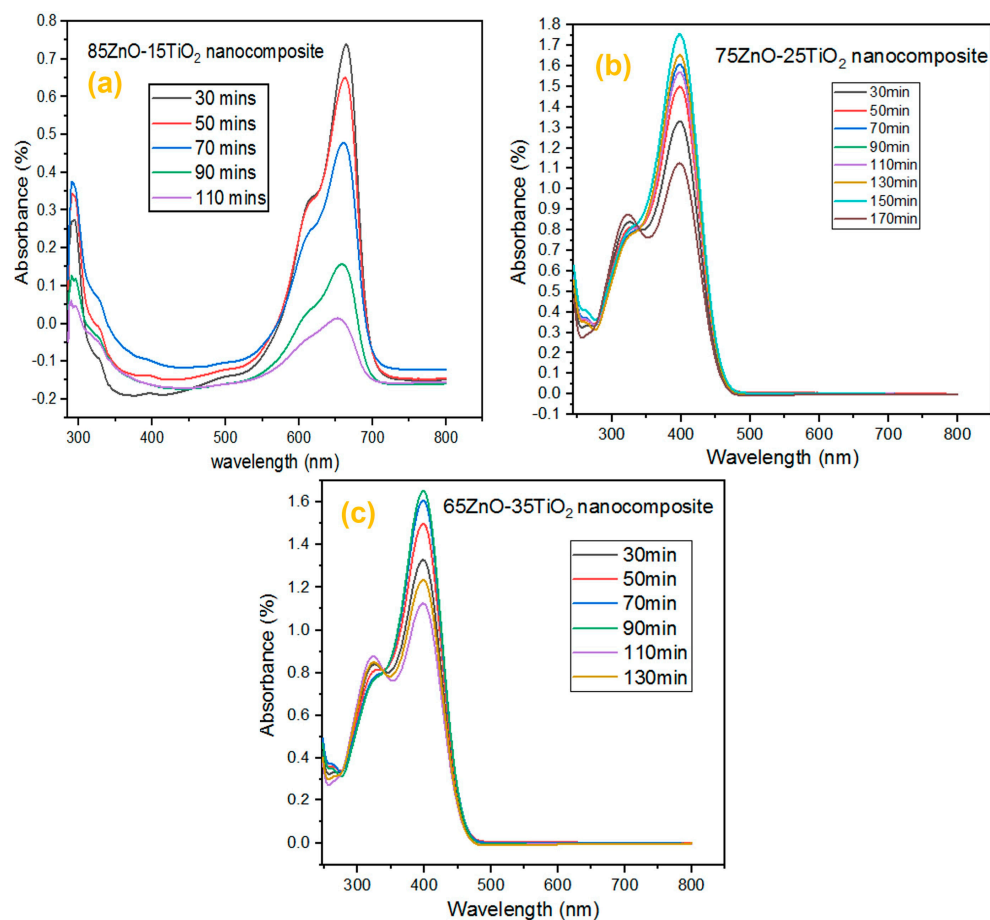
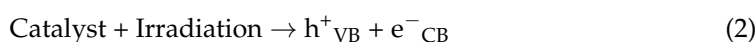
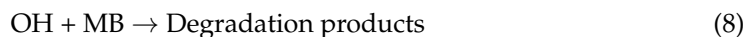


Figure 5. UV-visible absorption spectra of MB dye on ZnO/Zn₂TiO₄ nanocomposites surface: (a) 85% ZnO–15% Zn₂TiO₄ nanocomposite, (b) 75% ZnO–25% Zn₂TiO₄ nanocomposite, and (c) 65% ZnO–35% Zn₂TiO₄ nanocomposite.

The ZnO/Zn₂TiO₄ nanocomposites exhibit an increase in photocatalytic activity due to the synergistic interaction of Zn₂TiO₄ and ZnO. The design of the heterojunction because of the interfacial contact between ZnO and Zn₂TiO₄ may be the cause of this rising influence in catalytic activity. When a photocatalyst is exposed to radiation, the valence band and conduction band of the catalyst create a pair of positive holes and electrons. Positive photogenerated holes switch from Zn₂TiO₄ to the ZnO valence band. It causes the separation of positive holes and photoexcited electrons, which in turn increases the life of charge carriers. The OH radicals are produced when positive holes oxidize water molecules, while superoxide anions are produced when photoexcited electrons decrease dissolved oxygen molecules. The dye molecules are converted to inorganic by-products, by these OH radicals. The separation of positive holes and photoexcited electrons increase the production of OH radicals, which enhances the photocatalytic activity [41,42].

The following is a summary of the suggested mechanism:





It is clear that OH radicals were crucial in the methylene blue dye breakdown. The photonic crystal structure of ZnO/Zn₂TiO₄ has a great capacity for light harvesting, and its heterostructure has the ability to separate the photogenerated electron–hole pairs. The catalytic activity of the catalyst ZnO/Zn₂TiO₄ composites increases as a result of both of these characteristics. One of the factors that lowers the cost of the catalytic process is the recycling of the photocatalyst [43].

As seen in Figure 6a–d the effects of several experimental conditions including time, catalyst amount, dye concentration, and pH on the percentage of degradation were carefully evaluated. The photodegradation efficiency of methylene blue (MB) was calculated by using the following equation.

$$\text{Degradation (\%)} = C_e - C_0 / C_e \times 100 \quad (9)$$

where C_0 and C_e correspond to the initial and final concentration of dye before and after photoirradiation.

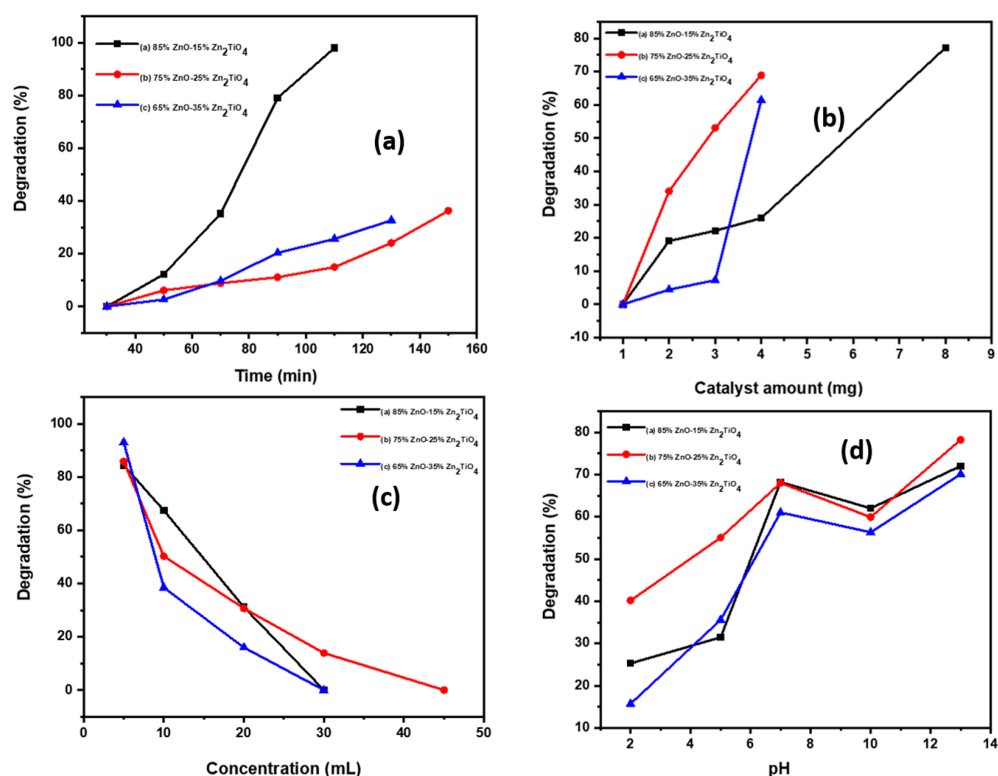


Figure 6. (a) Dye degradation (%) at various irradiation time intervals, (b) effect of catalyst amount on dye degradation (%), (c) effect of dye concentration on degradation (%), and (d) effect of pH on dye degradation (%).

The dye degradation properties of three ZnO/Zn₂TiO₄ nanocomposites on MB dye surface were investigated.

According to Figure 6a, the degrading effectiveness of the ZnO/Zn₂TiO₄ nanocomposites on MB dye were examined along with interval of time as, at 0–30 min, degradation percentage is zero, but with passing time through repeated intervals of 20 min, the percentage degradation goes on increasing. Nanocomposite “a” (at time 50 min, 70 min, 90 min, 110 min) percentage degradation goes on increasing to 5%, 35%, 70%, 80%, and 100% degradation. Nanocomposite “b” (at time 50 min, 70 min, 90 min, 110 min, 130 min, 150 min) percentage degradation goes on increasing to 6%, 8%, 12%, 15%, 25%, and 36% degrada-

tion. Nanocomposite “c” (at time 50 min, 70 min, 90 min, 110 min, 130 min) percentage degradation goes on increasing to 3%, 10%, 20%, 25%, and 34% degradation [34,35,44].

Figure 6b is used to demonstrate the removal effectiveness of MB dye with various catalyst amounts. The findings show that the percentage degradation efficiency rises with increasing catalyst amount of the three different ZnO/Zn₂TiO₄ nanocomposites when starting from 1 mg and using 30 mL of the MB dye solution. In nanocomposite “a”, increasing the amount from 2 to 8 mg increases the degradation percent (20–80%); in nanocomposite “b”, increasing the amount from 2 to 4 mg increases the degradation percent (33–70%); in nanocomposite “c”, increasing the amount from 2 to 5 mg increases the degradation percent (3–60%). The degradation percent efficiency goes on increasing, which could be attributed to an increase in the number of accessible adsorption sites on the catalyst surface [34].

When using ZnO/Zn₂TiO₄ nanocomposites, it was discovered that the percentage of degradation efficacy decreased as the concentration of dye increased. In nanocomposite “a”, increasing the concentration (5 mL, 20 mL, 35 mL, 50 mL) results in decreasing degradation (85%, 64%, 30%, 0%); in nanocomposite “b”, increasing the concentration (5 mL, 10 mL, 20 mL, 30 mL, 45 mL) results in decreasing degradation (85%, 45%, 25%, 10%, 0%); in nanocomposite “c”, increasing the concentration (5 mL, 20 mL, 30 mL, 45 mL) results in decreasing degradation (92%, 38%, 12%, 0%) as shown in Figure 6c. As a result of the Vander Waals contact between the catalyst and dye, there are fewer adsorption sites, which leads to degradation. The influence of the amount of catalyst on percentage degradation of dye (MB) efficacy was observed using a series of adsorption tests [34].

The pH directly affects the surface binding sites, surface charges, and structural characteristics of the dye molecule. As a result, the pH effect on percent dye degradation efficacy was observed by varying the solution pH from 2 to 13 using 0.1 M HCl and NaOH solutions, as shown in Figure 6d. Nanocomposite “a” at pH 7, 10, 13 had degradations of 68%, 62%, 70%. Nanocomposite “b” at pH 7, 10, 13 had degradations of 68%, 60%, 78%. Nanocomposite “c” at pH 7, 10, 13 had degradations of 60%, 57%, 70%. At low pH range, nanocomposite “a” at pH 2 and 5 had a degradation of 5% and 30%; in nanocomposite “b” at pH 2 and 5, there was degradation of 40% and 55%; in nanocomposite “c” at pH 2 and 4, there was degradation of 5% and 35%. Low pH to high pH increased the degradation efficiency, which may have caused the negative charge to decrease as a result of H⁺ neutralization. However, at pH levels higher than 7, some decrease may be as a result of increased competition between H⁺ and the dye.

Figure 7 shows the optical energy band gap of nanocomposites containing different ratios of ZnO and Zn₂TiO₄ (85% ZnO–15% Zn₂TiO₄, 75% ZnO–25% Zn₂TiO₄, and 65% ZnO–35% Zn₂TiO₄) was assessed utilizing the Kubelka-Munk function. The UV-visible data were utilized to calculate the bandgap of the synthesized nanocomposite. By analyzing the absorption edge in the UV spectrum and applying the formula $E_g \text{ (eV)} = 1240/\lambda$ [41–48], the estimated band gap serves as a key parameter for understanding the electronic structure. The calculated values of the band gap for the 85% ZnO–15% Zn₂TiO₄ nanocomposite, 75% ZnO–25% Zn₂TiO₄ nanocomposite, and the 65% ZnO–35% Zn₂TiO₄ nanocomposite are 3.15 eV, 3.25 eV, and 3.26 eV, respectively [49]. The broader absorbance maxima were used to calculate the band gap from each spectrum. The appearance of a negative charge on ZnO/Zn₂TiO₄ nanocomposites is compatible with the zeta potential results of the breakdown of dye molecules with various charges at various pH levels. As a result, it has been found that the degradation of dyes is extremely specific to the surface charge of the catalyst. Thus, ZnO/Zn₂TiO₄ nanocomposites may be categorized as ultrafast catalysts, which would be very beneficial for the quick and significant destruction of dangerous compounds [34,44].

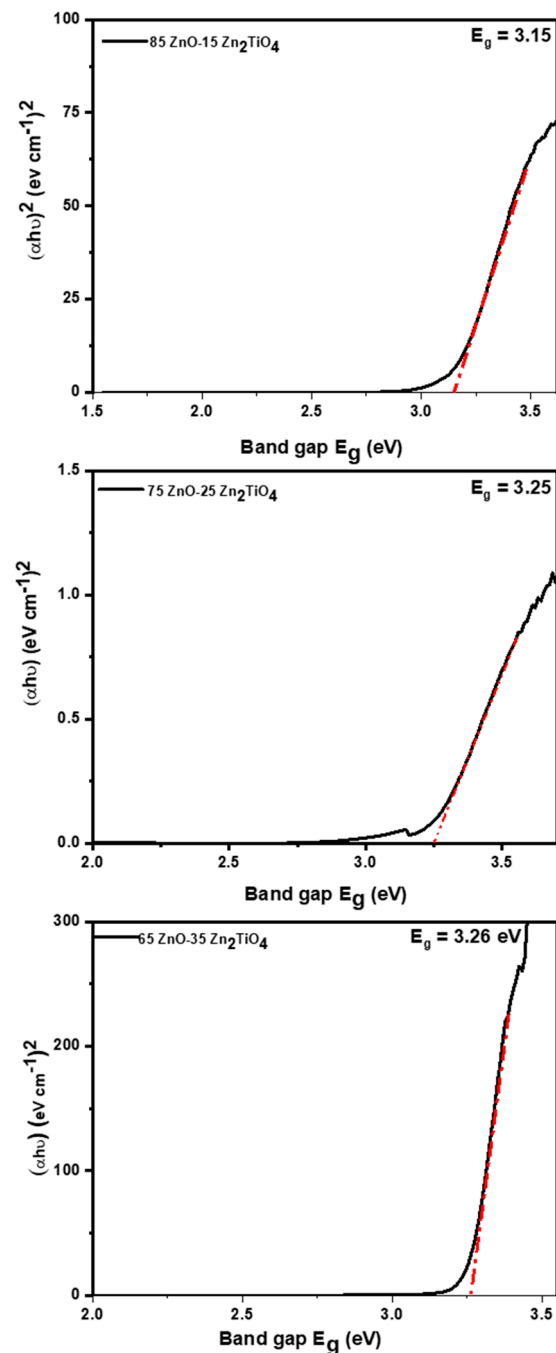


Figure 7. Optical energy bandgap of 85% ZnO–15% Zn₂TiO₄ nanocomposite, 75% ZnO–25% Zn₂TiO₄ nanocomposite, and 65% ZnO–35% Zn₂TiO₄ nanocomposite were evaluated using Kubelka-Munk function [39,40].

3. Experimental Details

3.1. Materials

In the present research work, zinc acetate (99% pure), titanium tetra-isopropoxide (99% pure), absolute ethanol, and distilled water were used. All chemicals were purchased from Sigma Aldrich (Karachi, Pakistan) with analytical grades.

3.2. Synthesis of ZnO/Zn₂TiO₄ Nanocomposites

Three nanocomposite compositions were produced using the sol–gel method: 85ZnO–15 Zn₂TiO₄, 75ZnO–25 Zn₂TiO₄, and 65ZnO–35 Zn₂TiO₄. Weighed amounts of Zn(CH₃COO)₂·H₂O powder (11.5 g, 9.8 g, and 7.6 g) were added to the mixture, which

was then agitated for 25 min at 40 °C. To synthesize the NaOH solution, we prepared three different concentrations: namely, 0.5 M, 0.75 M and 1.0 M at 40 °C. The $\text{Zn}(\text{CH}_3\text{COO})_2 \cdot 2\text{H}_2\text{O}$ solution was then added, and the mixture was agitated for approximately 140 min. The ZnO sol was formed once the stirring was completed. Meanwhile, 50-mL of ethanol was mixed with 5-mL, 10-mL, and 15-mL of titanium (IV) isopropoxide and agitated for 30 min to achieve homogeneity. After that, the solution was ionized with 20-mL of distilled water. Precipitation of $\text{ZnO}/\text{Zn}_2\text{TiO}_4$ was observed when the ZnO and Zn_2TiO_4 sols were combined and stirred for 250 min at 30 °C. The precipitate was then left for 25 h, filtered using filter paper, rinsed with distilled water, and dried at 150 °C overnight in an oven. Finally, the dried powder was calcined at 710 °C for 3 h.

3.3. Characterization

The SEM and EDX analysis were conducted using the FEI NOVA nano-SEM 450 (Hillsboro, OR, USA), which was equipped with an Oxford EDX detector (Abingdon, UK). X-ray diffraction measurements were performed using the Bruker D2 Phaser XRD model (Billerica, MA, USA). The FTIR spectrum of three $\text{ZnO}/\text{Zn}_2\text{TiO}_4$ nanocomposites was recorded in KBr using the FTIR-8400S instrument from Shimadzu (Kyoto, Japan), within the range of 4000–400 cm^{-1} . The absorption spectra and other photocatalytic measurements were obtained using the Shimadzu UV-2600 spectrophotometer, which is an ultraviolet–visible instrument.

4. Conclusions

The sol–gel technique was found to be an efficient, quick, easy, and inexpensive method for fabricating three $\text{ZnO}/\text{Zn}_2\text{TiO}_4$ nanocomposites. These nanocomposites were formed to study the degradation of methylene blue dye in the presence of sunlight. Various characterization methods, including XRD, EDX, UV-VIS, SEM, and FTIR, were used to investigate the physiochemical characteristics of the samples. FESEM observations revealed the formation of $\text{ZnO}/\text{Zn}_2\text{TiO}_4$ nanocomposites with a size range of 18–350 nm, resembling spread-out cotton packets. XRD measurements confirmed the formation of wurtzite ZnO and Zn_2TiO_4 structures in the three nanocomposites. UV spectra also confirmed the formation of the nanocomposites, showing two peaks for each sample. FTIR spectra further confirmed the formation of the nanocomposites, with peaks indicating Ti-O and Zn-O bond formations. The elemental composition of the nanocomposites was determined using energy dispersive X-ray spectroscopy, which revealed peaks for Ti, O, and Zn. Photocatalytic investigations were then carried out, analyzing the UV-visible absorption spectra of the dye on the nanocomposite surface, degradation of the dye at different irradiation time intervals and catalyst concentrations, and the influence of pH on dye degradation. The chemical synthesis of $\text{ZnO}/\text{Zn}_2\text{TiO}_4$ nanocomposites using the sol–gel method demonstrated its simplicity and ease of fabrication. This work obliges as an inspiration for young scientists to explore the potential applications of $\text{ZnO}/\text{Zn}_2\text{TiO}_4$ nanocomposites, particularly in photocatalytic activity studies.

Author Contributions: Conceptualization, M.H.; methodology, H.A.A. (Husnain Ahmad Abbasi); validation, H.A.A. (Habib Ahmad Abbasi) and S.S.; formal analysis, J.K. and M.U.H.; investigation, H.A.A. (Husnain Ahmad Abbasi) and M.A.K.; writing—original draft preparation, H.A.A. (Husnain Ahmad Abbasi) and M.H.; writing—review and editing, J.K. and M.M.A.M.; visualization, S.-K.C.; supervision, J.K.; project administration, M.H.; funding acquisition, M.M.A.M. All authors have read and agreed to the published version of the manuscript.

Funding: This research was funded by Princess Nourah bint Abdulrahman University Researchers Supporting Project number (PNURSP2024R56), Princess Nourah bint Abdulrahman University, Riyadh, Saudi Arabia.

Data Availability Statement: The original contributions presented in the study are included in the article, further inquiries can be directed to the corresponding author.

Acknowledgments: We are thankful to Princess Nourah bint Abdulrahman University for funding our project through Researchers Supporting Project number (PNURSP2023R56), Princess Nourah bint Abdulrahman University, Riyadh, Saudi Arabia.

Conflicts of Interest: The authors declare no conflicts of interest.

References

1. Bhanvase, B.A.; Shende, T.P.; Sonawane, S.H. A review on graphene–TiO₂ and doped graphene–TiO₂ nanocomposite photocatalyst for water and wastewater treatment. *Environ. Technol. Rev.* **2017**, *6*, 1–14. [[CrossRef](#)]
2. Roco, M.C.; Mirkin, C.A.; Hersam, M.C. Nanotechnology research directions for societal needs in 2020: Summary of international study. *J. Nanoparticle Res.* **2011**, *13*, 897–919. [[CrossRef](#)]
3. Khalid, A.; Ahmad, P.; Alharth, A.I.; Muhammad, S.; Khandaker, M.U.; Faruque, M.R.I.; Ud Din, I.; Alotaibi, M.A. A practical method for incorporation of Fe (III) in Titania matrix for photocatalytic applications. *Mater. Res. Express* **2021**, *8*, 045006. [[CrossRef](#)]
4. Wu, T.; Liu, X.; Liu, Y.; Cheng, M.; Liu, Z.; Zeng, G.; Shao, B.; Liang, Q.; Zhang, W.; He, Q.; et al. Application of QD-MOF composites for photocatalysis: Energy production and environmental remediation. *Coord. Chem. Rev.* **2020**, *403*, 213097. [[CrossRef](#)]
5. Raza, A.; Ikram, M.; Aqeel, M.; Imran, M.; Ul-Hamid, A.; Riaz, K.N.; Ali, S. Enhanced industrial dye degradation using Co doped in chemically exfoliated MoS₂ nanosheets. *Appl. Nanosci.* **2020**, *10*, 1535–1544. [[CrossRef](#)]
6. Raza, A.; Qumar, U.; Haider, A.; Naz, S.; Haider, J.; Ul-Hamid, A.; Ikram, M.; Ali, S.; Goumri-Said, S.; Kanoun, M.B. Liquid-phase exfoliated MoS₂ nanosheets doped with p-type transition metals: A comparative analysis of photocatalytic and antimicrobial potential combined with density functional theory. *Dalton Trans.* **2021**, *50*, 6598–6619. [[CrossRef](#)]
7. Wang, L.L.; Ren, Z.Q.; Li, Q. Improvement in optical and electrical properties of ZnO films by neodymium and aluminum co-doping. *J. Mater. Sci. Mater. Electron.* **2014**, *25*, 2992–2997. [[CrossRef](#)]
8. Yang, L.; Si, Z.; Weng, D.; Yao, Y. Synthesis, characterization and photocatalytic activity of porous WO₃/TiO₂ hollow microspheres. *Appl. Surf. Sci.* **2014**, *313*, 470–478. [[CrossRef](#)]
9. Yu, X.; Marks, T.J.; Facchetti, A. Metal oxides for optoelectronic applications. *Nat. Mater.* **2016**, *15*, 383–396. [[CrossRef](#)] [[PubMed](#)]
10. Serpone, N.; Emeline, A.V.; Ryabchuk, V.K.; Kuznetsov, V.N.; Artem'ev, Y.M.; Horikoshi, S. Why do hydrogen and oxygen yields from semiconductor-based photocatalyzed water splitting remain disappointingly low? Intrinsic and extrinsic factors impacting surface redox reactions. *ACS Energy Lett.* **2016**, *1*, 931–948. [[CrossRef](#)]
11. Sharma, P.K.; Dutta, R.K.; Pandey, A.C. Doping dependent room-temperature ferromagnetism and structural properties of dilute magnetic semiconductor ZnO: Cu²⁺ nanorods. *J. Magn. Magn. Mater.* **2009**, *321*, 4001–4005. [[CrossRef](#)]
12. Kryshtab, T.G.; Khomchenko, V.S.; Papusha, V.P.; Mazin, M.O.; Tzyrkunov, Y.A. Thin ZnS: Cu, Ga and ZnO: Cu, Ga film phosphors. *Thin Solid Films* **2002**, *403*, 76–80. [[CrossRef](#)]
13. Majumder, D.D.; Banerjee, R.; Ulrichs, C.H.; Mewis, I.; Goswami, A. Nano-materials: Science of bottom-up and top-down. *IETE Tech. Rev.* **2007**, *24*, 9–25.
14. Özgür, Ü. A comprehensive review of ZnO materials and devices. *J. Appl. Phys.* **2005**, *98*, 11. [[CrossRef](#)]
15. Li, Y.; Men, Y.; Kong, X.; Gao, Z.; Han, L.; Li, X. Enhanced electrical properties of ZnO transparent conducting films prepared by electron beam annealing. *Appl. Surf. Sci.* **2018**, *428*, 191–198. [[CrossRef](#)]
16. Vaidyanathan, R.; Kalishwaralal, K.; Gopalram, S.; Guronathan, S. RETRACTED: Nanosilver—The burgeoning therapeutic molecule and its green synthesis. *Biotechnol. Adv.* **2009**, *27*, 924–937. [[CrossRef](#)] [[PubMed](#)]
17. Peng, Y.; Xu, A.W.; Deng, B.; Antonietti, M.; Cölfen, H. Polymer-controlled crystallization of zinc oxide hexagonal nanorings and disks. *J. Phys. Chem. B* **2006**, *110*, 2988–2993. [[CrossRef](#)]
18. Koziej, D.; Lauria, A.; Niederberger, M. 25th anniversary article: Metal oxide particles in materials science: Addressing all length scales. *Adv. Mater.* **2014**, *26*, 235–257. [[CrossRef](#)]
19. Baruah, S.; Dutta, J. Hydrothermal growth of ZnO nanostructures. *Sci. Technol. Adv. Mater.* **2009**, *10*, 013001. [[CrossRef](#)]
20. Morkoç, H.; Özgür, U. *Zinc Oxide: Fundamentals, Materials and Device Technology*; John Wiley & Sons: Hoboken, NJ, USA, 2008.
21. Wang, Z.L. ZnO nanowire and nanobelt platform for nanotechnology. *Mater. Sci. Eng. R Rep.* **2009**, *64*, 33–71. [[CrossRef](#)]
22. Muller, S.; von Wenckstern, H.; Breitenstein, O.; Lenzner, J.; Grundmann, M. Microscopic Identification of Hot Spots in Multibarrier Schottky Contacts on Pulsed Laser Deposition Grown Zinc Oxide Thin Films. *IEEE Trans. Electron Devices* **2012**, *59*, 536–541. [[CrossRef](#)]
23. Klingshirn, C. ZnO: From basics towards applications. *Phys. Status Solidi B* **2007**, *244*, 3027–3073. [[CrossRef](#)]
24. Hameed AS, H.; Karthikeyan, C.; Ahamed, A.P.; Thajuddin, N.; Alharbi, N.S.; Alharbi, S.A.; Ravi, G. In vitro antibacterial activity of ZnO and Nd doped ZnO nanoparticles against ESBP producing Escherichia coli and Klebsiella pneumoniae. *Sci. Rep.* **2016**, *6*, 24312. [[CrossRef](#)] [[PubMed](#)]
25. Djurišić, A.B.; Leung, Y.H.; Tam, K.H.; Ding, L.; Ge, W.K.; Chen, H.Y.; Gwo, S. Green, yellow, and orange defect emission from ZnO nanostructures: Influence of excitation wavelength. *Appl. Phys. Lett.* **2006**, *88*, 103107. [[CrossRef](#)]
26. Djurišić, A.B.; Leung, Y.H. Optical properties of ZnO nanostructures. *Small* **2006**, *2*, 944–961. [[CrossRef](#)] [[PubMed](#)]
27. Xu, M.; Fujita, D.; Kajiwara, S.; Minowa, T.; Li, X.; Takemura, T.; Iwai, H.; Hanagata, N. Contribution of physicochemical characteristics of nano-oxides to cytotoxicity. *Biomaterials* **2010**, *31*, 8022–8031. [[CrossRef](#)] [[PubMed](#)]

28. Przybyszewska, M.; Zaborski, M. The effect of zinc oxide nanoparticle morphology on activity in crosslinking of carboxylated nitrile elastomer. *Express Polym. Lett.* **2009**, *3*, 542–552. [[CrossRef](#)]
29. Costa, B.C.; Rodrigues, E.A.; Tokuhara, C.K.; Oliveira RC, D.; Lisboa-Filho, P.N.; Rocha, L.A. ZnO nanoparticles with different sizes and morphologies for medical implant coatings: Synthesis and cytotoxicity. *BioNanoScience* **2018**, *8*, 587–595. [[CrossRef](#)]
30. Fujishima, A.; Rao, T.N.; Tryk, D.A. Titanium dioxide photocatalysis. *J. Photochem. Photobiol. C Photochem. Rev.* **2000**, *1*, 1–21. [[CrossRef](#)]
31. Monmaturapoj, N.; Sri-On, A.; Klinsukhon, W.; Boonnak, K.; Prahsarn, C. Antiviral activity of multifunctional composite based on TiO₂-modified hydroxyapatite. *Mater. Sci. Eng. C* **2018**, *92*, 96–102. [[CrossRef](#)]
32. Ibhaddon, A.O.; Fitzpatrick, P. Heterogeneous photocatalysis: Recent advances and applications. *Catalysts* **2013**, *3*, 189–218. [[CrossRef](#)]
33. Linsebigler, A.L.; Lu, G.; Yates, J.T., Jr. Photocatalysis on TiO₂ surfaces: Principles, mechanisms, and selected results. *Chem. Rev.* **1995**, *95*, 735–758. [[CrossRef](#)]
34. Khalid, A.; Ahmad, P.; Khan, A.; Khandaker, M.U.; Kebaili, I.; Alam, M.M.; Ud Din, I.; Muhamad, S.; Razzaq, Z.; Ur Rehman, I.; et al. Cytotoxic and photocatalytic studies of hexagonal boron nitride nanotubes: A potential candidate for wastewater and air treatment. *RSC Adv.* **2022**, *12*, 6592–6600. [[CrossRef](#)] [[PubMed](#)]
35. Asadzadeh Patehkhori, H.; Fattahi, M.; Khosravi-Nikou, M. Synthesis and characterization of ternary chitosan–TiO₂–ZnO over graphene for photocatalytic degradation of tetracycline from pharmaceutical wastewater. *Sci. Rep.* **2021**, *11*, 24177. [[CrossRef](#)]
36. Sanusi, I.J. Synthesis, Characterization, and Analysis of TiO₂/ZnO Composites Thin Films Photocatalysts for Ethanol Vapor Oxidation. Ph.D. Thesis, Miami University, Oxford, OH, USA, 2021.
37. Landge, V.K.; Huang, C.M.; Hakke, V.S.; Sonawane, S.H.; Manickam, S.; Hsieh, M.C. Solar-Energy-Driven Cu-ZnO/Zn₂TiO₄ Nanocomposite Photocatalyst for the Rapid Degradation of Congo Red Azo Dye. *Catalysts* **2022**, *12*, 605. [[CrossRef](#)]
38. Jagtap, S.; Priolkar, K.R. Chemical, Evaluation of ZnO nanoparticles and study of ZnO–TiO₂ composites for lead free humidity sensors. *Sens. Actuators B Chem.* **2013**, *183*, 411–418. [[CrossRef](#)]
39. Chivukula, V.; Ciplys, D.; Shur, M.; Dutta, P. ZnO nanoparticle surface acoustic wave UV sensor. *Appl. Phys. Lett.* **2010**, *96*, 233512. [[CrossRef](#)]
40. Pavasupree, S.; Ngamsinlapasathian, S.; Nakajima, M.; Suzuki, Y.; Yoshikawa, S. Hydrothermal synthesis, characterization, photocatalytic activity and dye-sensitized solar cell performance of mesoporous anatase TiO₂ nanopowders. *J. Photochem. Photobiol. A Chem.* **2008**, *43*, 149–157. [[CrossRef](#)]
41. Zhang, X.; Zhang, H.; Li, C.; Wang, K.; Sun, X.; Ma, Y. Recent advances in porous graphene materials for supercapacitor applications. *RSC Adv.* **2014**, *4*, 45862–45884. [[CrossRef](#)]
42. Lin, L.; Yang, Y.; Men, L.; Wang, X.; He, D.; Chai, Y.; Zhao, B.; Ghoshroy, S.; Tang, Q. A highly efficient TiO₂@ ZnO n–p–n heterojunction nanorod photocatalyst. *Nanoscale* **2013**, *5*, 588–593. [[CrossRef](#)]
43. Momeni, M.M.; Ghayeb, Y. Visible light-driven photoelectrochemical water splitting on ZnO–TiO₂ heterogeneous nanotube photoanodes. *J. Appl. Electrochem.* **2015**, *45*, 557–566. [[CrossRef](#)]
44. Lian, G.; Zhang, X.; Si, H.; Wang, J.; Cui, D.; Wang, Q. Boron nitride ultrathin fibrous nanonets: One-step synthesis and applications for ultrafast adsorption for water treatment and selective filtration of nanoparticles. *ACS Appl. Mater. Interfaces* **2013**, *5*, 12773–12778. [[CrossRef](#)]
45. Upadhyay, G.K.; Rajput, J.K.; Pathak, T.K.; Kumar, V.; Purohit, L.P. Synthesis of ZnO: TiO₂ nanocomposites for photocatalyst application in visible light. *Vacuum* **2019**, *160*, 154–163. [[CrossRef](#)]
46. Lachom, V.; Poolcharuansin, P.; Laokul, P. Preparation, characterizations and photocatalytic activity of a ZnO/Zn₂TiO₄ nanocomposite. *Mater. Res. Express* **2017**, *4*, 035006. [[CrossRef](#)]
47. Haghghatzaadeh, A.; Hosseini, M.; Mazinani, B.; Shokouhimehr, M. Improved photocatalytic activity of ZnO–TiO₂ nanocomposite catalysts by modulating TiO₂ thickness. *Mater. Res. Express* **2019**, *6*, 115060. [[CrossRef](#)]
48. Ibanez, J.G.; Gomez, F.; Konik, I.; Lozano, D.E.; Mugica, A.; Mesa, C.G.; Singh, M.M.; Szafran, Z.; Pike, R.M. Preparation of Semiconducting Materials in the Laboratory. Part 2. Microscale Chemical Bath Deposition of Materials with Band Gap Energies in the UV, Vis, and IR. *J. Chem. Edu.* **1997**, *74*, 1205–1207. [[CrossRef](#)]
49. Chandekar, K.V.; Shkir, M.; AlFaify, S. Tuning the optical band gap and magnetization of oleic acid coated CoFe₂O₄ NPs synthesized by facile hydrothermal route. *Mater. Sci. Eng. B* **2020**, *259*, 114603. [[CrossRef](#)]

Disclaimer/Publisher’s Note: The statements, opinions and data contained in all publications are solely those of the individual author(s) and contributor(s) and not of MDPI and/or the editor(s). MDPI and/or the editor(s) disclaim responsibility for any injury to people or property resulting from any ideas, methods, instructions or products referred to in the content.